Slow-structural relaxation in the metal–nonmetal transition range of liquid mercury: I. Experimental evidence

2001 J. Phys.: Condens. Matter 13 10293

(http://iopscience.iop.org/0953-8984/13/46/303)

INSTITUTE OF PHYSICS PUBLISHING JOURNAL OF PHYSICS: CONDENSED MATTER

J. Phys.: Condens. Matter **13** (2001) 10293–10305 PII: S0953-8984(01)25596-9

Slow-structural relaxation in the metal–nonmetal transition range of liquid mercury: I. Experimental evidence

H Kohno[1] **and M Yao**

Department of Physics, Graduate School of Science, Kyoto University, Sakyo-ku 606-8502, Kyoto, Japan

E-mail: yao@scphys.kyoto-u.ac.jp

Received 7 June 2001, in final form 6 September 2001
Published 2 November 2001
Online at stacks.iop.org/JPhysCM/13/10293

Abstract

The sound absorption coefficient, α, of expanded liquid mercury has been measured by means of the ultrasonic pulse-echo method at 20, 32 and 44 MHz in the temperature and pressure range up to 1600 °C and 210 MPa. Besides the critical attenuation, we have observed the secondary maximum in the density dependence of α/f^2 around 9 g cm^{-3}, where the metal–nonmetal (M–NM) transition occurs. When the frequency increases, the secondary maximum of α/f^2 tends to be smaller, which suggests that some kind of relaxation process takes place in the M–NM transition range of liquid mercury. We have separated the observed sound attenuation into the critical attenuation and the anomalous attenuation in the M–NM transition region utilizing the difference of the frequency dependence between the two components. Assuming a Debye-type relaxation model for the relaxation process due to the M–NM transition, we have estimated the relaxation time, τ, and the relative strength of the relaxation, $\beta_r/\beta_0 \equiv (\beta_0 - \beta_\infty)/\beta_0$, where β_0 and β_∞ are the adiabatic compressibility in the low-frequency and the high-frequency limit, respectively. The resultant τ is about 2 ns and almost independent of density. On the other hand, β_r/β_0 depends on density and has a broad maximum (∼4%) around 8.5 g cm^{-3}.

1. Introduction

The liquid–gas critical point of mercury is located at 1478 °C and 167 MPa [1]. Experimental studies on mercury in the wide density range including the supercritical region have revealed that liquid Hg is transformed to a semiconducting state around 8 to 9 g cm^{-3} [2], which is intermediate between the critical density (5.8 g cm^{-3}) and the density at the melting point (13.6 g cm^{-3}).

[1] JSPS Research Fellow.

0953-8984/01/4610293+13$30.00

Recently, we have measured the sound absorption coefficient, α, of expanded liquid Hg at 20 MHz and found two kinds of anomalous behaviour [3]. One is the critical attenuation, which is commonly observed in various systems [4], and the other is an anomalous increase of α around 9 g cm^{-3}, where the metal–nonmetal (M–NM) transition occurs. A similar observation has been reported subsequently by Kozhevnikov *et al* [5]. In the M–NM transition region, a secondary maximum in the density dependence of α appears around 8.5 g cm^{-3}. In contrast to the critical attenuation, the height of the maximum is almost independent of temperature at constant densities. It is known that the sound attenuation in simple liquids is given by a sum of the thermal conductivity term, the shear viscosity term and the bulk viscosity term [6]. From the viscosity data [7] we have estimated the shear viscosity contribution to be negligibly small. We have also estimated the thermal conductivity from the electrical conductivity data [8] by using the Wiedemann–Franz relation [9], which reveals that the sound attenuation is too large to be interpreted by the thermal conductivity term alone. Hence, it has been concluded that the secondary maximum of α in the M–NM transition range should be caused mainly by the anomalous increase of the bulk viscosity. Assuming a Debye-type relaxation for the frequency-dependent adiabatic compressibility, we have estimated the lower and upper limits of the relaxation time and predicted that the relaxation time should be of the order of nanoseconds, which is considerably longer than a typical time scale (∼picosecond [10]) of the single particle motion in the liquid state. Then it is suggested that slow dynamics should be generated by the sound pressure in the M–NM transition range.

Various mechanisms have been proposed to explain the anomalous increase in the bulk viscosity and most of them are concerned with the relaxation in some kind of two-state system [11]. Conventionally, the increase in the sound attenuation is explained by a simple model in which the increase in the bulk viscosity is attributed to the volume change between the two states [11]. If we apply the conventional model to the present Hg problem, however, the relative volume change, $\Delta V/V$, would be larger than 30%, which seems to be unphysically large. Thus, we must take into account the change in the electronic properties due to the M–NM transition [3].

In the present paper, we report the sound absorption coefficient, α, of liquid Hg at 32 and 44 MHz and analyse the data together with our previous data at 20 MHz [3]. The first purpose of this paper is to confirm that the frequency dependence of α in the M–NM transition range is consistent with the Debye-type relaxation model. The second purpose is to separate the observed α into the critical attenuation and the anomalous attenuation due to the M–NM transition more rigorously. The third purpose is to estimate the characteristic time of the relaxation process accurately in the M–NM transition range.

2. Experimental procedure

The sound velocity, v, and the sound absorption coefficient, α, of liquid mercury have been measured at 32 and 44 MHz in the temperature and pressure range up to 1600 °C and 210 MPa. The measurements were carried out using a sapphire sample cell which is the same as that described in our previous paper [3]. Single crystalline sapphire rods of 8 mm diameter were used as buffer rods for transmitting the ultrasonic waves. Two sapphire rods were inserted into a single crystalline sapphire tube with an inner diameter of 8 mm and outer diameter of 10 mm. The axial length of both the sapphire rods was 89 mm. A gap between the two rods was the sample part and the sample lengths l_s were 0.5 mm for the measurements at 32 MHz and 0.4 mm at 44 MHz. The cell assembly together with two heaters were set in an internally heated steel high-pressure vessel which was pressurized with argon gas. The temperature of the sample part was monitored by two W–5%Re:W–26%Re thermocouples.

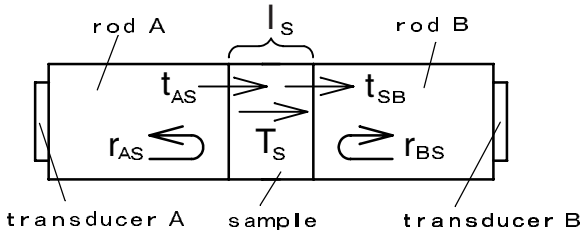

Figure 1. Schematic diagram of the sample cell. T_S is the transmission rate through the sample with a thickness of l_S. Definitions of the transmissivity, t_{IJ}, and the reflectivity, r_{IJ}, at the interfaces are also shown.

The schematic diagram of the sample cell is shown in figure 1. The sound velocity, v, was measured by an ultrasonic pulse transmission/echo method [12, 13]. Z-cut $Pb(Zr \cdot Ti)O_3$ transducers were bonded to the cold ends of the sapphire rods. We used the third harmonics for both frequencies.

The sound absorption coefficient α can be deduced from

$$\alpha = -\frac{\ln T_S}{l_S} \tag{1}$$

where T_s is the transmission rate through the sample. In contrast to the ambient conditions, where T_s can be measured by varying the sample thickness l_s, it is difficult to change l_s *in situ* under high temperature and pressure. Hence, we have estimated the transmission rate $T_S(A \rightarrow B)$ through the sample from A to B using the following equation:

$$T_S(A \rightarrow B) = \frac{V_{AB}}{\sqrt{V_{AA}V_{BB}}} \frac{\sqrt{|r_{AS}||r_{BS}|}}{|t_{AS}||t_{SB}|} \sqrt{\frac{\alpha_B \beta_A}{\alpha_A \beta_B}}. \tag{2}$$

Similarly, the transmission rate from B to A, $T_S(B \rightarrow A)$, is expressed as

$$T_S(B \rightarrow A) = \frac{V_{BA}}{\sqrt{V_{AA}V_{BB}}} \frac{\sqrt{|r_{AS}||r_{BS}|}}{|t_{BS}||t_{SA}|} \sqrt{\frac{\alpha_A \beta_B}{\alpha_B \beta_A}}. \tag{3}$$

Here V_{AB} (V_{BA}) is the voltage of the sound pulse which is transmitted through the rod A (B), the sample and the rod B (A) successively and reaches the transducer B (A). V_{AA} (V_{BB}) is the voltage of the echo signals reflected from the interface between the Hg sample and the buffer rods A (B) (see figure 1). r_{AS} (r_{BS}) is the reflectivity of the sound pressure at the interface between the buffer rod A (B) and the liquid sample and t_{AS} (t_{SB}) is the transmissivity. Both r_{AS} (r_{BS}) and t_{AS} (t_{SB}) can be calculated from the acoustic impedance [14], which is the product of the density and the sound velocity. α_A (α_B) is the efficiency of the transducer A (B) in converting the electric voltage to the sound pressure and β_A (β_B) is the efficiency in the inverse process. The last term in equations (2) and (3), $\sqrt{\alpha_B \beta_A / \alpha_A \beta_B}$, was determined by equating

$$T_S(A \rightarrow B) = T_S(B \rightarrow A). \tag{4}$$

Further details of the present method have been described elsewhere [3, 15]. The upper limit of the absolute error of α is evaluated to be 20% throughout the present paper. The method for estimation of the error has been described in our previous paper [3].

The temperatures and the pressures at which the measurements were carried out are shown in figure 2, where the bold line denotes the saturated vapour pressure curve terminated by the liquid–gas critical point and the thin lines show the isochore lines at every 1.0 g cm^{-3} [16].

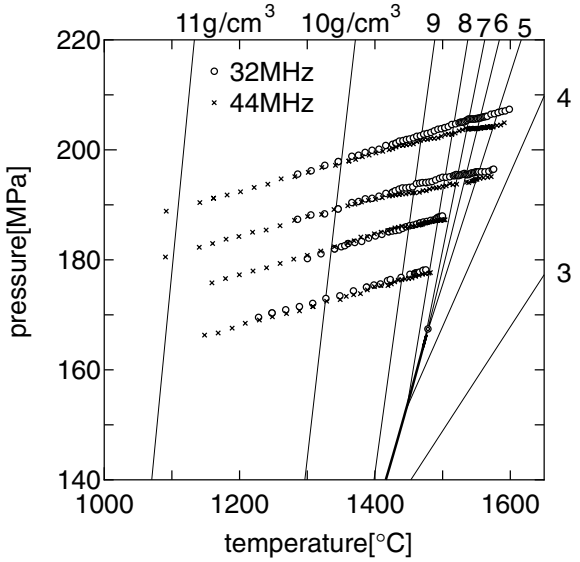

Figure 2. State points at which the measurements were carried out. Two different symbols are used depending on the frequency. The bold and thin lines denote the liquid–vapour coexistence curve and the isochore lines at every 1.0 g cm^{-3}, respectively.

Two different symbols are used depending on the frequency. The temperature was calibrated by using a saturated vapour pressure curve [16]. The experimental errors in temperature and pressure were ±5 °C and ±0.5 MPa, respectively.

3. Results

3.1. Sound velocity

The results of the sound velocity at 20 MHz have already been reported in our previous paper [3]. In the present paper, we have measured the sound velocity at 32 and 44 MHz. In accordance with the previous results at 20 MHz we have observed an inflection in the density dependence of the sound velocity at 32 and 44 MHz around 9 g cm^{-3}. The inflection was first discovered by Suzuki *et al* [12] and confirmed in subsequent studies [3, 13, 17–19]. Comparison of the present results at 32 and 44 MHz with the previous results at 20 MHz indicates no appreciable dispersion within the experimental uncertainties.

3.2. Sound attenuation

In figures 3(a)–(d), the sound absorption coefficient, α, at 32 and 44 MHz is plotted along several experimental paths shown in figure 2 as a function of temperature. The symbols in figure 3 correspond to those in figure 2. The pressure at which the experimental path crosses the isochore line of 9 g cm^{-3} is shown in the figure. The error bars show the absolute error which is estimated from the uncertainties of the transmission rate and the sample thickness [3]. The relative error, which can be seen from the scattering of the data points, is much smaller than the error bars. At temperatures below 1400 °C, α increases slowly with temperature and begins to rise at higher temperatures. The slope of α becomes the steepest on approaching a temperature

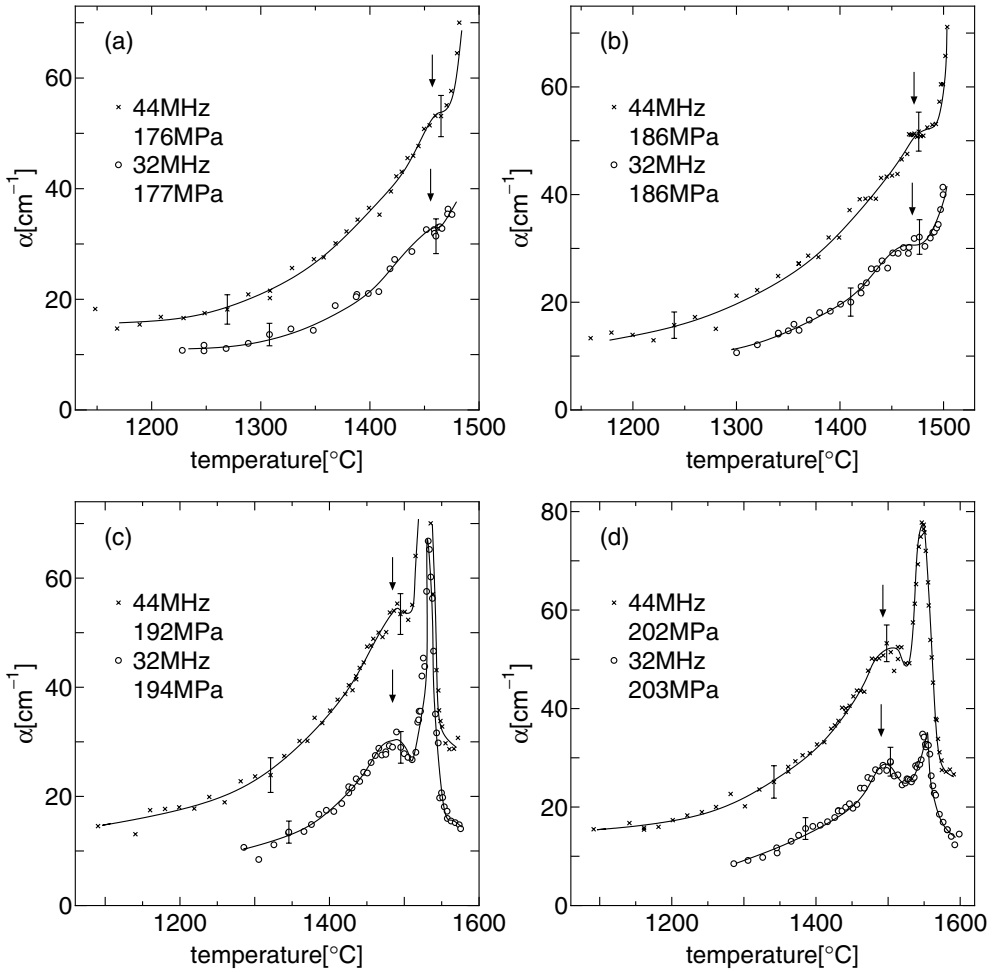

Figure 3. The sound absorption coefficient, α, at 32 MHz ($\circ$) and 44 MHz ($\times$) along several experimental paths shown in figure 2 is plotted as a function of temperature. The pressures at which the experimental path crosses the isochore line of 9 g cm^{-3} are shown in the figure. The arrows in the figure indicate the secondary maximum of α. The solid lines in the figures are a guide for the eyes.

corresponding to the critical density, though the peak is not attained in figures 3(a) and (b) because α is too large to be measured. We could reach the peaks at pressures much higher than the critical pressure. In figure 3(c), α at 32 MHz has a peak value of 66.8$\pm$12.0 cm^{-1} at 1532 °C. In figure 3(d), α at 32 and 44 MHz has peak values of 34.8$\pm$7.0 and 77.8$\pm$15.6 cm^{-1}, respectively, at 1547$\pm$1 °C. Beside the critical attenuation there appears a shoulder around 1470 °C in the temperature dependence of α, as shown by the arrows in figures 3(a) and (b). At higher pressures, where the critical attenuation is reduced, the shoulder is resolved from the critical attenuation and becomes a clear secondary maximum around 1500 °C, as shown by the arrows in figures 3(c) and (d).

Since the density is the most relevant parameter for the M–NM transition, we re-plot α near 186 MPa at 32 and 44 MHz (see figure 3(b)) together with α at 20 MHz [3] as a function

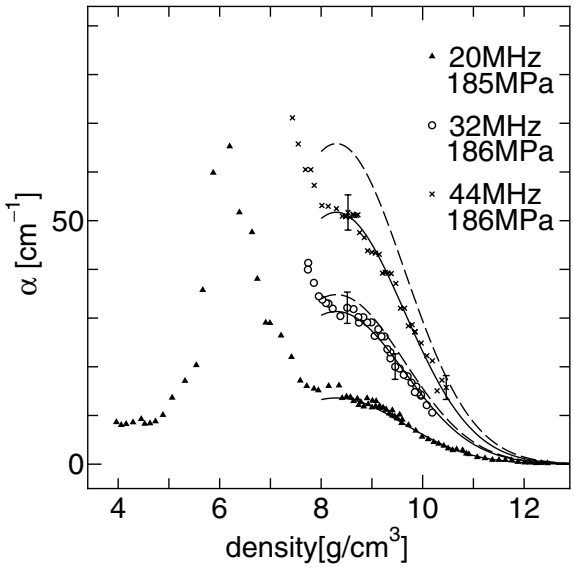

Figure 4. The sound absorption coefficient, α, at 20 (▲), 32 (○) and 44 MHz (×) near 186 MPa is plotted as a function of density. The data at 20 MHz are taken from our previous paper [3]. The dashed lines denote the variations of α expected for 32 and 44 MHz from the f^2-dependence when α at 20 MHz is taken as a standard. The solid lines denote the density dependence of α at 20, 32 and 44 MHz calculated from equation (9) by using the density dependence of β_r/β_0 shown by the solid line in figure 9 with $\tau = 2.2$ ns.

of density in figure 4. It should be noted that the secondary maximum or a hump is located in the M–NM transition range (8–9 g cm^{-3}) irrespective of the frequency.

We plot α at 20 MHz as a function of pressure at constant densities (7.0–10.0 g cm^{-3}) in figure 5. The pressure dependence of α at 32 and 44 MHz is qualitatively similar to that at 20 MHz in the common density range. At higher densities, α is small and the pressure dependence is almost flat. When the density decreases from 8.0 g cm^{-3}, α increases and begins to depend on pressure and the slope becomes considerably larger around 180 MPa. Using the present results and the thermal pressure coefficient [16], $(\partial P/\partial T)\rho$, we can deduce the temperature coefficient, $-(1/\alpha)(\partial\alpha/\partial T)\rho$, which is useful to discuss the mechanism of sound attenuation. At 180 MPa, $-(1/\alpha)(\partial\alpha/\partial T)\rho$ at 9.0, 8.0 and 7.0 g cm^{-3} are estimated to be $(1.7\pm0.3)\times10^{-3}$, $(5.6\pm1.1)\times10^{-3}$ and $(5.0\pm1.0)\times10^{-2}$ K^{-1}, respectively. It should be underlined that $-(1/\alpha)(\partial\alpha/\partial T)\rho$ itself varies depending on pressure or temperature at densities lower than 8.0 g cm^{-3}. At 7.0 g cm^{-3}, for example, $-(1/\alpha)(\partial\alpha/\partial T)\rho$ at 200 MPa is about one half of that at 180 MPa. These findings suggest that the observed α is little affected by the critical attenuation at densities higher than 8.0 g cm^{-3} since critical attenuation depends strongly on temperature.

4. Discussion

In the hydrodynamic regime the sound absorption coefficient of simple liquids should be proportional to the square of the frequency f [6]. In figure 4 we take the data of α at 20 MHz as a standard and the values of α expected for 32 and 44 MHz from the f^2-dependence are shown by the dashed lines in the density region above 8 g cm^{-3}. It should be noted that the

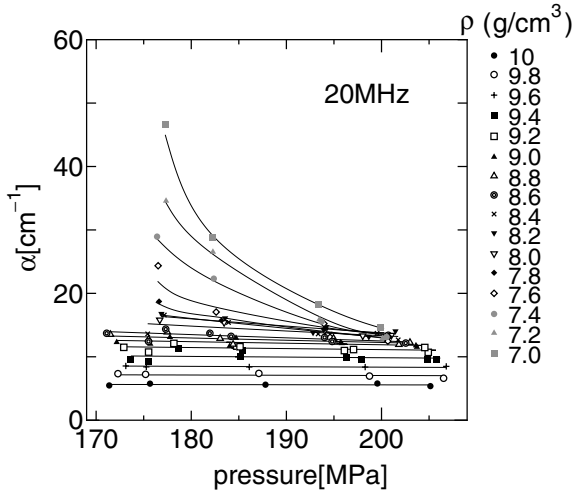

Figure 5. The sound absorption coefficient, α, at 20 MHz is plotted as a function of pressure at constant densities. Several different symbols are used depending on the density ρ. The thin lines in the figure are a guide for the eyes.

experimentally observed values of α deviate downward from the dashed lines in the M–NM transition range and that the discrepancy grows with frequency. This finding strongly suggests that some kind of relaxation process should take place in the M–NM transition range of Hg.

In this section, we separate the observed α into the critical attenuation α^{CP} and the attenuation due to the relaxation in the M–NM transition range, $\alpha^{\mathrm{M-NM}}$, in the following three density regions. Here we use the data at 200 MPa (see figure 6), because the critical attenuation is not significantly large.

4.1. The density region between 8 and 10 g cm^{-3}

At densities higher than 8 g cm^{-3}, α^{CP} is negligibly small (see figure 5). Moreover, at densities lower than 10 g cm^{-3}, the shear viscosity and thermal conductivity contribution to α/f^2 are very small compared to the bulk viscosity term [3]. Hence α at densities between 8 and 10 g cm^{-3} can be expressed as

$$\frac{\alpha}{f^2} \simeq \frac{\alpha^{\mathrm{M-NM}}}{f^2} = \frac{2\pi^2}{\rho v^3}\zeta \tag{5}$$

where ζ is the bulk viscosity, v is the sound velocity and ρ is the density. In general v and ζ are related to the frequency-dependent adiabatic compressibility, $\beta(\omega)$, as [11],

$$v^2 = \frac{\mathrm{Re}(1/\beta(\omega))}{\rho} \tag{6}$$

$$\zeta = \frac{\mathrm{Im}(1/\beta(\omega))}{\omega} \tag{7}$$

where ω is the angular frequency ($=2\pi f$).

Assuming a simple Debye relaxation model for $\beta(\omega)$

$$\beta(\omega) = \beta_\infty + \frac{\beta_0 - \beta_\infty}{1 + \mathrm{i}\omega\tau} \tag{8}$$

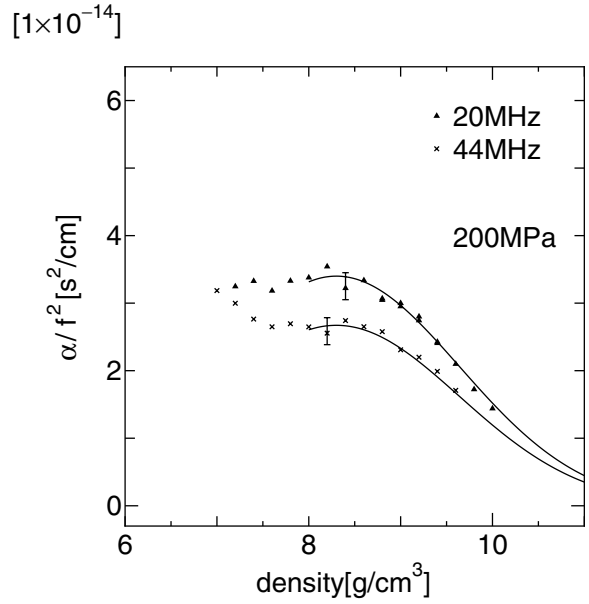

Figure 6. The sound absorption coefficient divided by the square of the frequency, α/f^2, at 200 MPa for 20 MHz (▲) and 44 MHz (×) is plotted against the density. The solid lines denote the smoothed variations of α/f^2. Typical error bars are shown in the figure.

one can introduce the relaxation time τ which is a measure of the delay time for the volume change after the application of the sound pressure. Here β_0 is the static adiabatic compressibility and β_∞ is the adiabatic compressibility at frequencies beyond the radio frequency range. The static adiabatic compressibility can be expressed as $\beta_0 = 1/\rho v_0^2$, where v_0 is the sound velocity at the low frequency limit. Putting equations (8) into equation (7), we obtain the expression for ζ. By combining this with equation (5), α/f^2 can be expressed as

$$\frac{\alpha}{f^2} \simeq \frac{2\pi^2}{\rho v^3}\zeta = \frac{2\pi^2}{\rho v^3}\frac{(\beta_0 - \beta_\infty)\tau}{\beta_0^2 + \omega^2\tau^2\beta_\infty^2}. \tag{9}$$

By putting equation (8) into equation (6), the sound velocity can be expressed as

$$v^2 = \frac{1}{\rho}\left(\frac{1}{\beta_0} + \frac{\beta_0 - \beta_\infty}{\beta_\infty\beta_0}\frac{\beta_\infty^2\omega^2\tau^2}{\beta_0^2 + \beta_\infty^2\omega^2\tau^2}\right). \tag{10}$$

Then we try to deduce β_0, β_∞ and τ at densities higher than 8.0 g cm^{-3} by using equations (9) and (10) with the data for α at 20 and 44 MHz and v at 20 MHz [3]. In figure 7, τ deduced from the data points in figure 6 is plotted against the density using open circles. At densities between 8.0 and 9.6 g cm^{-3}, τ is 2.2±0.3 ns and has no appreciable dependence on density. This result confirms our early prediction that τ should lie between 0.1 and 8 ns [3]. In figure 8, the deduced β_0 and β_∞ are plotted against the density using open circles and triangles, respectively. Both β_0 and β_∞ increase with decreasing density. The dashed line shows $\beta_v \equiv 1/\rho v^2$ at 20 MHz, which is smaller than β_0 by about 0.3%, as shown in the inset of figure 8. The difference in v between 20 and 44 MHz can be calculated from the estimated β_0, β_∞ and τ, and it proves to be very small (<0.5%), which is consistent with the experimental

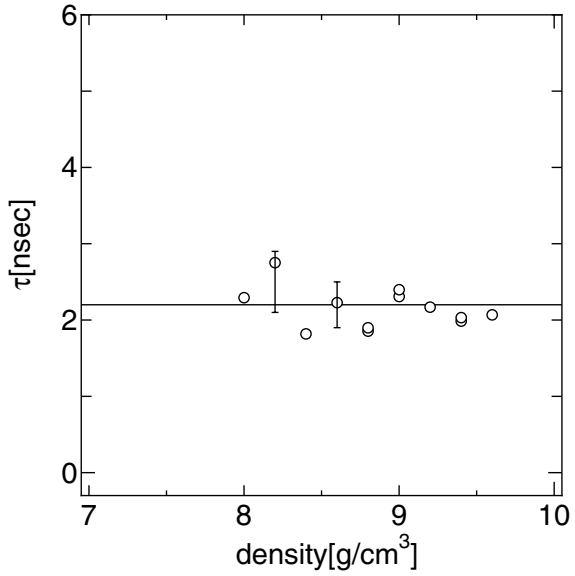

Figure 7. The relaxation time, τ, deduced from the sound velocity and the sound absorption coefficient at 200 MPa shown in figure 6 is plotted against the density using open circles. Typical error bars are shown in the figure. The solid line denotes $\tau = 2.2$ ns.

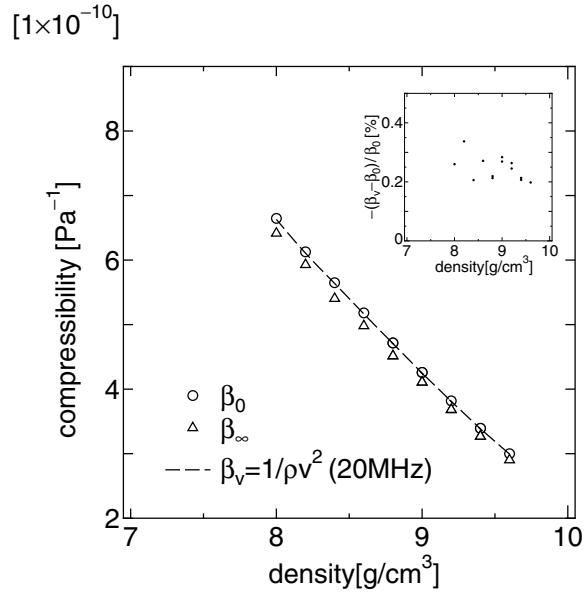

Figure 8. The values of β_0 (○) and β_∞ (△) deduced from the sound velocity and the sound absorption coefficient at 200 MPa are shown plotted against the density. The variation of $\beta_v \equiv 1/\rho v^2$ calculated from v at 20 MHz is shown by the dashed line. The inset shows the density dependence of the relative difference between β_0 and β_v, $-(\beta_v - \beta_0)/\beta_0$.

result that no appreciable dispersion was observed. In figure 9, the relative relaxation intensity defined by $\beta_r/\beta_0 \equiv (\beta_0 - \beta_\infty)/\beta_0$ is plotted using open circles. A broad maximum (about 4%)

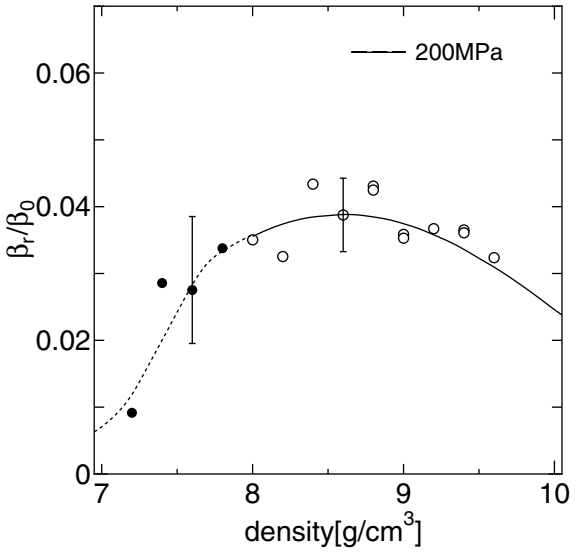

Figure 9. The relative relaxation intensity, $\beta_r/\beta_0 \equiv (\beta_0 - \beta_\infty)/\beta_0$, is plotted against the density. The open circles denote β_r/β_0 deduced from equations (9) and (10) with the data points in figure 6. The solid line shows the density dependence of β_r/β_0 deduced from the smoothed variations of α/f^2 in figure 6 with constant τ (2.2 ns). The full circles denote β_r/β_0 deduced from α^{M-NM}/f^2 which is separated from the total α/f^2 (see the text). The dotted line is a guide for the eyes.

seems to appear in the density dependence of β_r/β_0. The solid line denotes the density dependence of β_r/β_0 deduced from the smoothed variations of α/f^2 shown in figure 6 with constant τ (=2.2 ns).

In order to ascertain the validity of the Debye relaxation, we calculate α at various frequencies by using the parameters β_0, β_∞ and τ and compare them with the experimental results at different pressures. In figure 4, the solid lines denote the density dependence of α at 20, 32 and 44 MHz calculated from equation (9) by using the density dependence of β_r/β_0 shown by the solid line in figure 9 with $\tau = 2.2$ ns. The agreement between the calculated and experimental values of α is fairly good.

4.2. The density region between 7 and 8 g cm^{-3}

Since the critical attenuation becomes important below 8.0 g cm^{-3}, we try to separate α into α^{CP} and α^{M-NM} utilizing the difference of their frequency dependence. Theoretical studies on the critical phenomena have predicted that the critical attenuation per wavelength, α_λ^{CP}, should be expressed as a function of the dimensionless frequency [4],

$$\omega^* = \frac{\omega}{2\Gamma_\xi}. \tag{11}$$

Here Γ_ξ is the decay rate of the entropy fluctuation and can be written as

$$\Gamma_\xi = D\xi^{-2} \tag{12}$$

where ξ is the correlation length and D is the thermal diffusivity. In the low frequency limit $\omega/\Gamma_\xi \ll 1$ (i.e. hydrodynamic regime), α_λ^{CP} is proportional to ω/Γ_ξ [4]. In the high frequency case $\omega/\Gamma_\xi \gg 1$, however, ξ exceeds the thermal diffusion length and the perturbed thermal

equilibrium cannot be restored within the period of the sound wave. Thus the frequency dependence of α_λ^{CP} should be suppressed compared to the linear dependence on ω. In the marginal case $\omega/\Gamma_\xi \approx 1$, α_λ^{CP} on the critical isochore is given as about 0.05 from the scaling function [20].

Since the experimental value of $\alpha_\lambda (=\alpha_\lambda^{CP} + \alpha_\lambda^{M-NM})$ is about 0.05 at 7.0 g cm^{-3} (see figure 6), α_λ^{CP} alone is smaller than 0.05 at 7.0 g cm^{-3} and even smaller at higher densities. Furthermore, when one moves away from the critical region, Γ_ξ increases and the hydrodynamic regime is extended to a wider frequency range. Thus, we may assume that α_λ^{CP} is simply proportional to ω (i.e. $\alpha^{CP} \propto f^2$) in the density range between 7.0 and 8.0 g cm^{-3}. As for α^{M-NM}, we adopt the following simplified expression for the Debye-type relaxation,

$$\frac{\alpha^{M-NM}}{f^2} \simeq \frac{2\pi^2}{v}\frac{\beta_r}{\beta_0}\frac{\tau}{1+\omega^2\tau^2} \tag{13}$$

because β_r is much smaller than β_∞, as shown in the previous section. Hence the total sound attenuation can be written as

$$\frac{\alpha}{f^2} = \frac{\alpha^{M-NM}}{f^2} + \frac{\alpha^{CP}}{f^2} = \frac{A}{1+\omega^2\tau^2} + B. \tag{14}$$

At densities from 8.0 to 9.6 g cm^{-3}, τ has been estimated to be about 2.2 ns and nearly constant.Assuming that τ is also independent of density even at lower densities, we determine the density-dependent parameters A and B in equation (14) in such a way that the experimental data at different frequencies shown in figure 6 can be reproduced. In figure 9, the resultant values of β_r/β_0 are plotted against the density by full circles. The error bar shows the uncertainty corresponding to $\tau = 2.2\pm0.3$ ns. When the density decreases from 8.0 to 7.0 g cm^{-3}, β_r/β_0 decreases rapidly to zero, as shown by the dotted line which is a guide for the eyes.

4.3. Critical region

At densities lower than 7.0 g cm^{-3}, α can be simply expressed as

$$\frac{\alpha}{f^2} \simeq \frac{\alpha^{CP}}{f^2}. \tag{15}$$

The density dependence of α^{CP}/f^2 at 20 MHz is shown along several experimental paths in figure 10, in which α^{CP}/f^2 at densities between 7.0 to 8.0 g cm^{-3} is deduced in the last section. The pressure at which the experimental path crosses the critical isochore line is shown in the figure. The large increase of the sound attenuation is observed near the critical density and the peak becomes smaller as the pressure increases. More detailed discussion about the dynamic critical phenomena will be presented by us in another paper [21].

5. Summary

The sound absorption coefficient, α, of expanded liquid mercury has been measured by means of the ultrasonic pulse–echo method at 20, 32 and 44 MHz. The measurements have been carried out in the temperature and pressure range up to 1600 °C and 210 MPa. In addition to the critical attenuation, we have observed a secondary maximum in the density dependence of α around 9 g cm^{-3}, where the M–NM transition occurs. The frequency dependence of the secondary maximum suggests the existence of a relaxation process in the

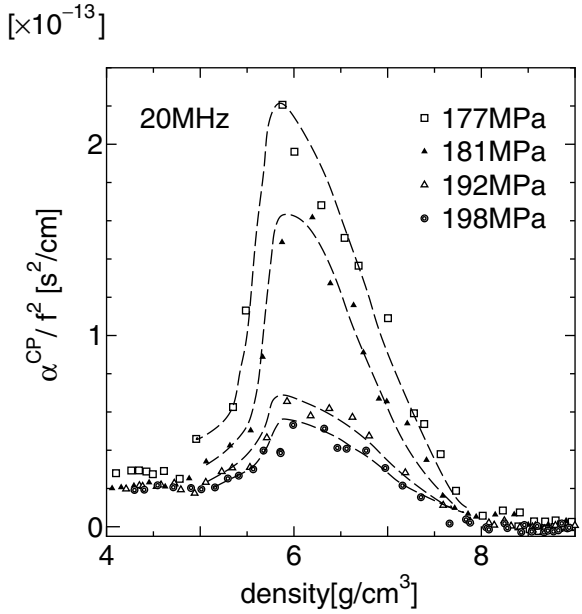

Figure 10. The critical attenuation, α^{CP}/f^2, at 20 MHz along several experimental paths is shown as a function of the density. The pressure at which the experimental path crosses the critical isochore line is shown in the figure. Several different symbols are used depending on the pressure. The dashed lines in the figure are a guide for the eyes.

M–NM transition range. The critical attenuation is important only in the density range below 8.0 g cm^{-3}. We have separated the observed sound attenuation into the critical attenuation and the secondary maximum, utilizing the difference of the frequency dependence between the two components. Assuming a Debye-type relaxation for the frequency-dependent adiabatic compressibility, we have estimated the relaxation time to be about 2 ns in the M–NM transition region. In a subsequent paper [22], we will suggest a simple model in which the change of the electronic state in the M–NM transition region is taken into account and tentatively calculate the relaxational part of the compressibility in order to explain the anomalous sound attenuation in the M–NM transition range qualitatively.

Acknowledgments

The authors are grateful to Messrs Y Kajihara, Y Hiejima, N Itokawa and Miss I Hirano for collaboration on the experiments. We also thank Professors F Hensel and A Onuki for valuable discussions and helpful advice. This work was partially supported by a Grant-in-Aid for Scientific Research from the Ministry of Education, Science, Sports and Culture, Japan.

References

[1] Hensel F and Warren W W Jr 1999 *Fluid Metals* (Princeton, NJ: Princeton University Press) ch 1
[2] Hensel F and Warren W W Jr 1999 *Fluid Metals* (Princeton, NJ: Princeton University Press) ch 4 and references therein
[3] Kohno H and Yao M 1999 *J. Phys.: Condens. Matter* **11** 5399

[4] Kawasaki K 1976 *Phase Transitions and Critical Phenomena* vol 5a, ed C Domb and M S Green (London: Academic) ch 4
[5] Kozhevnikov V F, Arnold D I, Briggs M E, Naurzakov S P, Viner J M and Taylor P C 1999 *J. Acoust. Soc. Am.* **106** 3424
[6] Landau L D and Lifshitz E M 1963 *Fluid Mechanics* (Oxford: Pergamon) ch 8
[7] Tippelskirch H v, Franck E U and Hensel F 1975 *Ber. Bunsenges. Phys. Chem.* **79** 889
[8] Yao M and Endo H 1982 *J. Phys. Soc. Japan* **51** 966
[9] Kittel C 1986 *Introduction to Solid State Physics* 6th edn (New York: Wiley) ch 6
[10] Hansen J-P and McDonald I R 1986 *Theory of Simple Liquids* 2nd edn (London: Academic) p 217
[11] Litovitz T A and Davis C M 1965 *Physical Acoustics* vol II, ed W P Mason (New York: Academic) ch 5
[12] Suzuki K, Inutake M, Fujiwaka S, Yao M and Endo H 1980 *J. Physique Coll.* **41** C8 66
[13] Yao M, Okada K, Aoki T and Endo H 1996 *J. Non-Cryst. Solids* **205–207** 274
[14] Truell R, Elbaum C and Chick B B 1969 *Ultrasonic Methods in Solid State Physics* (New York: Academic) ch 2
[15] Yao M, Itokawa N, Kohno H, Kajihara Y and Hiejima Y 2000 *J. Phys.: Condens. Matter* **12** 7323
[16] Götzlaff W 1988 *PhD Thesis* University of Marburg
[17] Kozhevnikov V F, Naurzakov S P and Arnold D I 1993 *J. Moscow Phys. Soc.* **3** 191
[18] Okada K, Odawara A and Yao M 1998 *Rev. High Pressure Sci. Technol.* **7** 736
[19] Dladla B S, Pilgrim W-C and Hensel F 1997 *Z. Phys. Chem.* **199** 295
[20] Onuki A 1997 *Phys. Rev.* E **55** 403
[21] Kohno H and Yao M in preparation
[22] Kohno H, Yao M and Hensel F in preparation